Structural Equilibrium of DNA Represented with Different Force Fields

Michael Feig and B. Montgomery Pettitt

Department of Chemistry, University of Houston, Houston, Texas 77204-5641 USA

ABSTRACT   We have recently indicated preliminary evidence of different equilibrium average structures with the CHARMM and AMBER force fields in explicit solvent molecular dynamics simulations on the DNA duplex $d(C_5T_5) \cdot d(A_5G_5)$ (Feig, M. and B. M. Pettitt, 1997, Experiment vs. Force fields: DNA conformation from molecular dynamics simulations. *J. Phys. Chem. B.* 101:7361–7363). This paper presents a detailed comparison of DNA structure and dynamics for both force fields from extended simulation times of 10 ns each. Average structures display an A-DNA base geometry with the CHARMM force field and a base geometry that is intermediate between A- and B-DNA with the AMBER force field. The backbone assumes B form on both strands with the AMBER force field, while the CHARMM force field produces heterogeneous structures with the purine strand in A form and the pyrimidine strand in dynamical equilibrium between A and B conformations. The results compare well with experimental data for the cytosine/guanine part but fail to fully reproduce an overall B conformation in the thymine/adenine tract expected from crystallographic data, particularly with the CHARMM force field. Fluctuations between A and B conformations are observed on the nanosecond time scale in both simulations, particularly with the AMBER force field. Different dynamical behavior during the first 4 ns indicates that convergence times of several nanoseconds are necessary to fully establish a dynamical equilibrium in all structural quantities on the time scale of the simulations presented here.

INTRODUCTION

Molecular dynamics simulations of biological macromolecules have been established as a theoretical tool to help understand their structure, dynamics and function (McCammon and Harvey, 1987). Such calculations depend not only on initial conditions but also on the force fields. Refined force fields that describe the atomic interactions, parametrized using accurate experimental data and high quality calculations, have become available. Increased computer power allows for more significant simulation times, which provide more stringent tests of the methodology.

In molecular dynamics simulations of nucleic acids (Beveridge et al., 1994; Louise-May et al., 1996) the treatment of the long-range electrostatic interactions between the highly charged solute and an ionic environment has been a fundamental issue. The previous use of simple truncation schemes often did not provide for stable trajectories (Smith and Pettitt, 1991; Schreiber and Steinhauser, 1992). While the inclusion of smoothing functions in some cases has been successful (Ravishanker et al., 1997; Auffinger and Beveridge, 1995; Steinbach and Brooks, 1994), the Ewald summation technique (Ewald, 1921; de Leeuw et al., 1980; Smith and Pettitt, 1994) is more commonly used. A series of nanosecond molecular dynamics simulations of nucleic acid systems with Ewald summation, the longest over 5 ns, have been recently reported by several groups (Yang and Pettitt, 1996; Weerasinghe et al., 1995; Young et al., 1997; Duan et al., 1997; Cieplak et al., 1997; Cheatham et al., 1995;

Cheatham and Kollman, 1996; Auffinger and Westhof, 1996; Lee et al., 1995) demonstrating stable trajectories comparable to experimental data. However, similar simulations of $d(CGCGAATTCGCG)_2$ (Yang and Pettitt, 1996; Young et al., 1997; Cieplak et al., 1997) and $d(CCAACGTTGG)_2$ (Cheatham and Kollman, 1996) found final structures in B-DNA conformations with the AMBER program but in A-DNA with the CHARMM force field. This observation was attributed predominantly to a difference in the force fields (Cheatham and Kollman, 1996), but because of different simulation conditions, in particular a higher ionic concentration in the simulation with the CHARMM force field, a separation of the influence of the force field from the solution conditions, sequence, and other methodological differences was problematic.

A direct comparison between the latest published CHARMM (MacKerell, Jr. et al., 1995) and AMBER (Cornell et al., 1995) force fields from molecular dynamics simulations of the double-stranded DNA decamer $d(C_5T_5) \cdot d(A_5G_5)$ under otherwise identical simulation conditions illustrates their considerably different structures and dynamics (Feig and Pettitt, 1997). Although both force fields produce fluctuations on the nanosecond time scale between A- and B-like structures, the AMBER force field was found to generally prefer the B form, while the CHARMM force field produced mostly the A-DNA form. In this paper we present a detailed analysis of our simulations, now extended to 10 ns, to more fully assess both force fields in comparison with the experimental data.

The sequence $d(C_5T_5) \cdot d(A_5G_5)$ provides a test case for some of the major structural issues of right-handed double-stranded DNA. The homooligomeric cytosine/guanine and adenine/thymine moieties allow comparison of base specific structure with extensive experimental data on homopoly-

meric DNA. Particularly interesting is the preference of A/T basepairs for B conformations versus C/G basepairs for A conformations. In addition, bending of the double helix is expected to be introduced through the C-T junction.

Homopolymeric adenine/thymine tracts are biologically important as promoter elements for gene transcription (Boettcher, 1990; Schultes, 1991; Iyer and Struhl, 1995) and have been associated with intrinsic bending of DNA polymers (Koo et al., 1986; Haran et al., 1994; Hagerman, 1994). This is attributed to a particular structure, distinct from random sequence DNA, with a narrowed minor groove (Alexeev et al., 1987) and highly propeller-twisted basepairs (Nelson et al., 1987). Increased hydration compared to other sequences has been found from binding studies (Chalikian et al., 1994) and acoustical measurements (Buckin et al., 1989).

While earlier fiber x-ray diffraction studies on poly(dA) · poly(dT) inferred a heteronomous conformation with the adenine strand in A form and the thymine strand in B form (Arnott et al., 1983) recent single crystal studies of A/T tracts find B-DNA conformations on both strands (Nelson et al., 1987; DiGabriele et al., 1989; Edwards et al., 1992). However, the relation to the physiologically relevant solution structure is unclear (Fairall et al., 1989) because crystal packing forces (Dickerson et al., 1987; Jain and Sundaralingam, 1989; D. and Steitz, 1993; Dickerson et al., 1994) and dehydrating agents for crystallization (Sprous et al., 1995) have been shown to influence the molecular structure.

NMR measurements of poly(dA) · poly(dT) under solution conditions correlate with mostly B-DNA backbones with the furanose rings on both strands in C2′-endo (Behling and Kearns, 1986; Leijon et al., 1995) or thymine sugars in O4′-endo/C1′-exo and adenine sugars in C2′-endo (Celda et al., 1989; Searle and Wakelin, 1990) conformations. Raman experiments (Thomas and Peticolas, 1983; Taillandier et al., 1987) indicate parts of the thymine backbone in C3′-endo conformation particularly at lower temperatures of 0°C and higher salt concentrations. This suggests occasional rapid interconversion from C2′-endo to C3′-endo on the thymine backbone on a time scale that cannot be resolved with NMR. From resonance Raman studies (Jolles et al., 1985) it was concluded that the adenine strand of poly(dA) · poly(dT) adopts the A conformation, but this may be due to DNA polymer aggregation with a preference for A-DNA (Herbeck et al., 1976; Lindsay et al., 1988). The base geometries of poly(dA) · poly(dT) in solution, estimated from linear and circular dichroism studies, are described as "non-B" (Brahms and Brahms, 1990), but an A-type helix with a 3-Å rise, 20° base inclination, and non-zero roll and tilt of opposite signs was determined from recent pulsed electric linear dichroism experiments (Yamaoka et al., 1997).

The structure of homopolymeric cytosine/guanine segments differs significantly from adenine/thymine tracts, promoting the base sequence dependence of DNA conformation. In crystal diffraction experiments A-DNA is observed for both alternating and non-alternating cytosine/

guanine nucleotide sequences (McCall et al., 1985; Haran et al., 1987; Mooers et al., 1995), but influence of the crystal environment on the structures has also been found (Ramakrishnan and Sundaralingam, 1993).

Solution studies of poly(dG) · poly(dC), as well as short C/G nucleotides, with NMR and Raman both report A- and B-type backbone conformations (Benevides et al., 1986; Nishimura et al., 1986; Sarma et al., 1986; Rinkel et al., 1986; Wolk et al., 1989). In lower salt (0.1 M NaCl) and at higher temperatures B conformations are preferred (Benevides et al., 1986; Nishimura et al., 1986; Rinkel et al., 1986; Wolk et al., 1989), while A-DNA backbones were found at lower temperatures and higher salt concentration (Nishimura et al., 1986). In 1 M NaCl at 30° a heteronomous conformation with the guanine backbone in B-type O4′-endo and the cytosine backbone in A-type C3′-endo form has been deduced from NMR data (Nishimura et al., 1986). The observation of predominantly A-DNA backbones in poly(dG) · poly(dC) at 30–60°C in relatively low salt concentration (Sarma et al., 1986) could also be the result of polymer aggregation. Linear dichroism experiments of poly(dG) · poly(dC) support highly inclined bases, characteristic of A-DNA, with pronounced interbase buckle and propeller twist similar to poly(dA) · poly(dT) (Edmondson and Johnson, 1986; Kang and Johnson, 1994), but circular dichroism suggests base geometries intermediate between A and B forms (Wolk et al., 1989; Vorlickova et al., 1996).

The combination of a C/G tract with an A/T tract has been studied for $d(G_5T_5) \cdot d(A_5C_5)$ in 0.1 M NaCl and 6 M NaCl solution with Raman spectroscopy (Wang et al., 1989) and for $d(AC_5T_7G) \cdot d(CA_7G_5T)$ in water/trifluorethanol mixtures with circular dichroism (Ivanonv et al., 1996). Both report an A/B junction with the C/G part in A form and the A/T part in B form in high salt and high trifluorethanol concentrations, respectively, while the B conformation is observed throughout the sequences in low salt solutions.

In this work on $d(C_5T_5) \cdot d(A_5G_5)$ we first give the computational methods to generate the trajectories and review the methods of analysis. The results of the simulations using the two different force fields are then presented. We end with a discussion and comparison with experimental measures of structure.

METHODS

Starting from model-built canonical A-DNA (QUANTA, 1994) the decamer $d(C_5T_5) \cdot d(A_5G_5)$ (see Fig. 1) was simulated in the NVT ensemble at 300 K with the most recent published CHARMM and AMBER all-atom nucleic acid force fields (Cornell et al., 1995; MacKerell, Jr. et al., 1995). Solvation in 2285 explicit TIP3P (Jorgensen et al., 1983) water molecules, 18 Na⁺ counterions to balance the DNA charge, and 32 additional Na⁺/Cl⁻ ion pairs resulted in a simulation box of 4.0 × 4.0 × 5.0 nm. This corresponds to ion concentrations of 1.2 M Na⁺ and 0.8 M Cl⁻.

The simulation program was developed in this laboratory (Smith et al., 1996). It employs periodic boundary conditions, the velocity Verlet integration schemes (Allen and Tildesley, 1987), and the SHAKE algorithm (Ryckaert et al., 1977) to enforce holonomic constraints of all chemical bonds. An integration time step of 2 fs was used. Electrostatic interactions
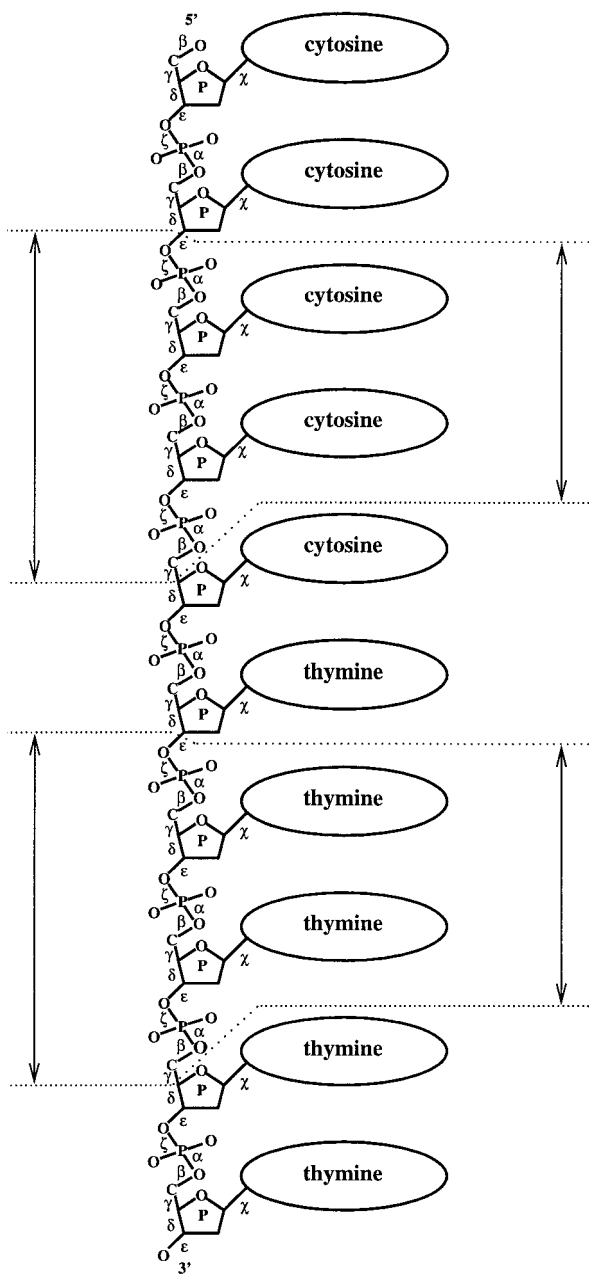
FIGURE 1 Basepairs and backbone dihedrals used for calculation of cytosine/guanine and thymine/adenine averages (see text), shown only for the first strand.

were calculated using a twin-range implementation of the exact Ewald summation (Smith and Pettitt, 1995). The direct contribution to the Ewald sum was calculated every time step within a first cutoff of 1.2 nm and updated every 10 steps from 1.2 nm to the second cutoff of 2.0 nm. A convergence factor α of 1.5 and 13 reciprocal space vectors in each direction achieved optimal performance.

Initial equilibration, described in detail elsewhere (Yang and Pettitt, 1996; Weerasinghe et al., 1995), includes an initial 20-step steepest descent minimization followed by alternating runs with either the solvent or the solute fixed and velocity reassignment every 50 steps from a canonical Maxwell distribution at 300 K for ~200 ps. Configurations were saved every 100 fs. All simulation runs were carried out on the Cray T3E parallel computer at Pittsburgh Supercomputing Center.

The analysis of DNA base geometries involves the determination of helical parameters, defined previously (Dickerson et al., 1989). The cal-

culation depends on the choice of a reference helical axis, which can be either local or global, with mathematical issues still under current discussion (Babcock et al., 1994; Babcock and Olson, 1994; El Hassan and Calladine, 1995). The most commonly used implementations are NEW-HEL93 (Dickerson, 1992) using a local helical axis, and the CURVES package (Lavery and Sklenar, 1988, 1989), which fits a global axis through the basepairs. Although the global axis approach focusing on the overall conformation rather than local conformation would be better suited for our analysis, the definition of a global helical axis for short DNA fragments less than a full helix turn (11–12 base pairs) is problematic (Lavery and Sklenar, 1989). Therefore we use the NEWHEL93 code to calculate the helical parameters in our analysis.

RESULTS

We continued the two previously reported simulations (Feig and Pettitt, 1997) with CHARMM and AMBER force fields to 10 ns for CHARMM and 6 ns and 10 ns for the AMBER force field. A second simulation with the AMBER force field was performed to investigate the reproducibility of a transition at 1.2 ns to an unusual "Z-like" local backbone conformation affecting local helix structure in the adenine tract (see below) in the first AMBER simulation. The second AMBER simulation was started with atomic coordinates from the first AMBER simulation at 1 ns, but with reassigned velocities, and continued to 10 ns without observing this backbone structure. Detailed results will be given only on the CHARMM and the second AMBER simulation. Because we saw the Z-like structure only once we cannot estimate an equilibrium population for it.

The simulated structures in all three simulations remained stable throughout the simulation time with all structural parameters in experimentally observed ranges except for the adenine backbone transition mentioned above. Average pressures after equilibrium were found to be -338.4 atm (± 304.3), -575.6 atm (± 296.4), and -568.2 atm (± 298.8) for the CHARMM and the first and second AMBER simulations. In Fig. 2 average structures calculated over the last 6 ns are shown for both force fields. An RMS deviation of 1.9 Å between both structures for all non-hydrogen atoms excluding the edge basepairs after aligning the principal axes of the moment of inertia tensor indicates overall comparable average structures with both force fields. More pronounced are differences in the backbone with an RMS deviations of 2.4 Å compared to only 1.0 Å for the base atoms.

While inclined bases in the CHARMM structure describe A-DNA features, the parallel arrangement of the basepairs in the AMBER structure indicate a B-like conformation with local inclination angles close to zero. The different orientation of the upper cytosine/guanine and lower thymine/adenine basepairs suggest a bent helical axis. Furthermore, a narrower major groove in the thymine/adenine tract of the AMBER simulation is apparent from the backbone shape.

The time series of the helical parameters inclination and rise in Fig. 3 confirm a general preference of CHARMM parameters for A-DNA, whereas the AMBER force field
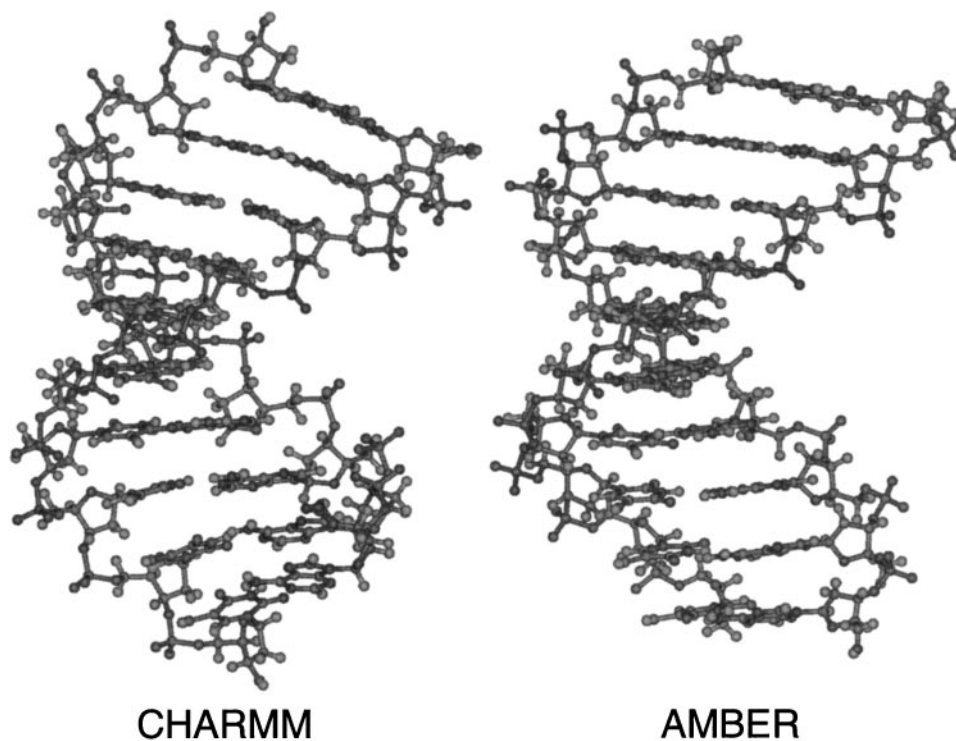
FIGURE 2 Average structures of d(C$_5$T$_5$) · d(A$_5$G$_5$) from CHARMM and AMBER simulations over the last 6-ns simulation time. Cytosine/guanine pairs are shown on the top, thymine/adenine on the bottom.

produces structures intermediate between canonical A and B-DNA forms. However, large amplitude fluctuations between A- and B-like conformations occur in both simulations. For the questions of convergence and sampling sufficiency this observation has important consequences. Previous simulations were considered converged after arriving at and oscillating around a stable conformation for an extended time period (Young et al., 1997). In the case of the simulations presented here, convergence has to be defined by achieving a dynamical equilibrium between the sampled A- and B-type conformations. A lower estimate for the convergence times can be found from the onset of frequent sugar repuckering from C3′-endo to C2′-endo conformations in the thymine and cytosine backbone during the CHARMM force field simulation only after 2 ns. In order to estimate convergence times for the helical parameters, we calculated RMS fluctuations within 2 ns averaging blocks shifted over the length of the trajectories. The most pronounced effect is found for fluctuations in base inclination angles during the AMBER simulation shown in Fig. 4. Up to 3.5 ns along the simulation time inclination angle values fluctuate significantly more within the 2-ns averaging blocks than during the remainder of the trajectory. Similar observations were also made in other structural parameters during the first nanoseconds of the simulations. While a more detailed analysis on DNA dynamics is in progress, for the purpose of this paper we will assume, based on the block average estimates, that the simulation trajectories from both force fields represent converged dynamical equilibria in all structural quantities after 4 ns and use only the last 6 ns for the following structural analysis and comparison.

In calculating undistorted structural averages over the homopolymeric moieties the two edge basepairs on either side as well as the C/T junction basepairs will be excluded. As shown in Fig. 2 the backbone angles (Saenger, 1984) are averaged starting from the second ϵ dihedral along the backbone until the γ dihedral of the fifth base, similarly for bases 6–9 and the opposite strand. Base-base and base-axis helical parameters are averaged for basepairs 3–4 and 7–8 and relative inter-basepair parameters for basepair steps 2–4 and 6–8.

Base geometries

Base geometries may be characterized by the average helical parameters. Table 1 compares the results for cytosine/guanine and thymine/adenine basepairs with experimental data on homopolymer tracts from x-ray diffraction, which provides the most detailed structural information. However, full agreement between simulation and experiment is not necessarily expected because of different solution and crystal environments. Average geometries were calculated for C/G and A/T basepairs from studies on d(C$_4$G$_4$)$_2$ (Haran et al., 1987), d(G$_4$C$_4$)$_2$ (McCall et al., 1985), d(CGCA$_5$GCG) · d(CGCT$_5$GCG) (Nelson et al., 1987), and d(CGCGA$_6$CG) · d(CGT$_6$CGCG) (Grzeskowiak et al., 1991), since x-ray data for the studied sequence d(C$_5$T$_5$) · d(A$_5$G$_5$) is not available. However, local DNA structure has been found to be predominantly determined by the central basepair step with only minor influence by the next neighboring basepairs from electrophoretic gel measurements (DeSantis et al.,
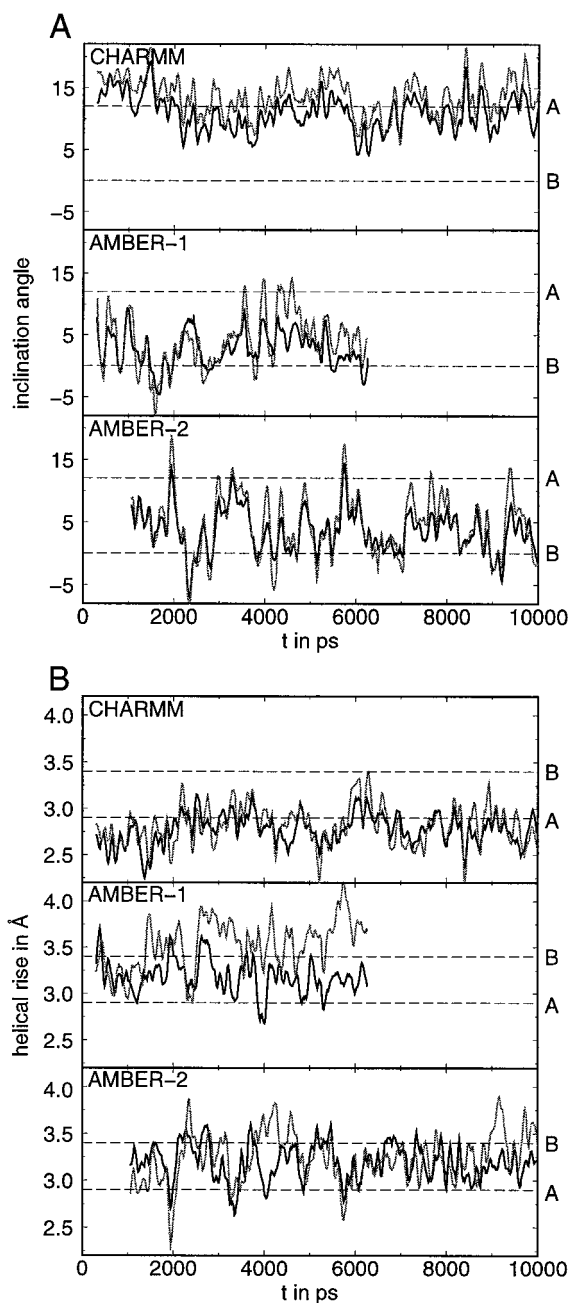
FIGURE 3   Base inclination (*A*) and helical rise (*B*) in CHARMM and AMBER simulations over the simulation times for cytosine/guanine (—) and thymine/adenine (· · ·) basepairs. Typical A and B values are given for comparison.
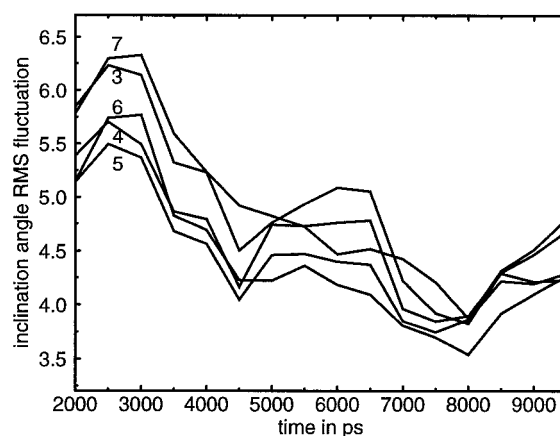

FIGURE 4   Base inclination angle root mean square fluctuations within 2-ns averaging blocks over the course of the AMBER simulation. Results are shown individually for the inner basepairs at the midpoint of the block interval.

experimental values the errors σ_{avg} are estimated from the standard deviation σ of the N averaged values as:

$$\sigma_{\mathrm{avg}} = \frac{\sigma}{\sqrt{N}} \tag{1}$$

TABLE 1   Average helical parameters compared to experimental results for cytosine/guanine and thymine/adenine basepairs

Geometry	Pair	CHARMM[*]	AMBER[*]	X-ray[#§]
Inclination	C/G	9.86 (0.26)	3.47 (0.11)	10.3 (1.7)
	T/A	12.61 (0.28)	5.15 (0.11)	−1.44 (0.4)
Tip	C/G	5.01 (0.10)	−0.82 (0.05)	3.84 (0.8)
	T/A	−2.58 (0.10)	−4.92 (0.08)	−0.66 (0.8)
x Displacement	C/G	−4.31 (0.02)	−3.89 (0.02)	−3.94 (0.13)
	T/A	−4.26 (0.04)	−2.98 (0.02)	−0.38 (0.10)
y Displacement	C/G	−0.21 (0.01)	0.80 (0.01)	0.17 (0.11)
	T/A	−0.03 (0.02)	0.87 (0.01)	0.63 (0.09)
Roll	C/G	4.16 (0.09)	3.18 (0.03)	5.7 (0.98)
	T/A	6.32 (0.08)	1.13 (0.06)	−0.9 (1.01)
Tilt	C/G	−1.67 (0.04)	−0.40 (0.01)	−1.7 (0.32)
	T/A	2.11 (0.04)	1.92 (0.03)	0.7 (0.27)
Slide	C/G	−1.77 (0.00)	−1.70 (0.01)	−1.5 (0.09)
	T/A	−1.43 (0.01)	−0.99 (0.01)	−0.1 (0.13)
Rise	C/G	2.75 (0.01)	3.20 (0.01)	2.97 (0.07)
	T/A	2.86 (0.01)	3.09 (0.01)	3.22 (0.08)
Twist	C/G	31.4 (0.03)	28.8 (0.04)	32.7 (0.95)
	T/A	32.3 (0.02)	32.1 (0.09)	36.1 (0.50)
Propeller	C/G	−3.21 (0.12)	−2.81 (0.06)	−11.8 (2.1)
	T/A	−11.60 (0.08)	−13.26 (0.11)	−21.4 (0.8)
Buckle	C/G	9.58 (0.08)	2.55 (0.14)	6.8 (0.7)
	T/A	10.79 (0.14)	−4.61 (0.16)	−1.6 (2.4)

Statistical errors are given in parentheses for simulation averages and experimental values.

[*]Averages are calculated over 4–10 ns, with NEWHELIX (Dickerson, 1992) without edge and junction basepairs. Distances are in nm.

[#]C/G values averaged over six inner basepairs from crystal structures for d(CCCCGGGG)$_2$ (Haran et al., 1987) and d(GGGGCCCC)$_2$ (McCall et al., 1985).

[§]A/T values averaged over eight inner basepairs from crystal structures for d(CGCA$_5$GCG) · d(CGCT$_5$GCG) (Nelson et al., 1987) and d(CGCGA$_6$CG) · d(CGT$_6$CGCG) (Grzeskowiak et al., 1991).

1990) and statistical analysis of crystal structures when properly normalized (Yanagi et al., 1991). Structural quantities for the three central C/G and T/A basepairs excluding the C-T junction and edge basepairs are thus expected to provide a good representation of homopolymeric C/G and T/A tracts. The same applies to the central C/G and T/A basepairs in the C/G and A/T tracts of the experimentally studied sequences.

Statistical errors of the average values are given in parentheses for all simulation and experimental values. For the

TABLE 2   Individual average base-axis and intrabase parameters in CHARMM simulation

Pair	Inclination	Tip	x Displacement	y Displacement	Propeller	Buckle
CG 2	8.3 (4.7)	6.6 (6.3)	−4.6 (0.72)	−0.32 (0.61)	−1.6 (7.4)	12.7 (9.2)
CG 3	9.3 (4.0)	5.7 (5.2)	−4.4 (0.68)	−0.20 (0.50)	−2.9 (6.7)	10.8 (8.3)
CG 4	10.5 (3.7)	4.3 (4.2)	−4.2 (0.64)	−0.22 (0.43)	−3.6 (6.7)	8.4 (8.1)
CG 5	11.3 (3.6)	2.9 (3.7)	−4.2 (0.63)	−0.39 (0.39)	−5.2 (6.5)	4.4 (7.6)
TA 6	12.1 (3.6)	−1.2 (4.0)	−4.3 (0.62)	−0.28 (0.45)	−7.5 (6.7)	8.9 (7.7)
TA 7	12.2 (3.9)	−2.6 (4.1)	−4.3 (0.68)	−0.10 (0.50)	−11.0 (6.8)	11.2 (8.9)
TA 8	13.1 (4.3)	−2.6 (4.5)	−4.2 (0.79)	0.04 (0.58)	−12.2 (6.9)	10.4 (9.8)
TA 9	14.1 (4.7)	−3.5 (5.7)	−4.0 (0.95)	0.14 (0.68)	−11.5 (7.9)	11.1 (12.0)

Standard deviations from all datapoints between 4 and 10 ns are given in parentheses.

To determine the error of the simulation averages we analyzed the standard deviations of block averages over the last 6 ns for different block sizes. For a statistically independent series of values the standard deviation of block averages is given by (1). If the values are correlated with each other the quantity $\sigma_{\text{block}} \cdot \sqrt{N}$ will increase with the averaging block size until a plateau value is reached at sufficiently large block sizes (Friedberg and Cameron, 1970; Jacucci and Rahman, 1984; Allen and Tildesley, 1987). However, this only results in sufficient statistical sampling and a simple extrapolation for the error at longer block sizes if no oscillatory behavior with periods longer than the initial correlation time is present. In this case $\sigma_{\text{block}} \cdot \sqrt{N}$ will show a more complex dependency on increasing block size reflecting the frequency spectrum of the studied quantity. Thus, for the structural quantities presented here, the estimation of the error in the average over the full analysis length from errors in block averages over shorter pieces of the trajectory becomes nontrivial. The error values presented here are estimated from this type of analysis, which will be presented elsewhere in more detail (M. Feig and B. M. Pettitt, in preparation).

Individual averages and root-mean-square fluctuations characterizing the dynamic range are listed in Tables 2–5 for each basepair for all datapoints between 4 and 10 ns from the CHARMM and AMBER simulations.

The inclination angle and displacement along the short (x) axis of the basepairs with respect to the helical axis, the relative horizontal and vertical displacements, slide and rise, and the relative twist angle between two successive basepairs are most distinctive between A- and B-type conformations. With the CHARMM force field both cytosine/guanine and thymine/adenine basepairs adopt, on average,

typical A-DNA values. Simulation with the AMBER force field produces an average structure intermediate between A- and B-DNA. Similar results are found for the cytosine/guanine part in the AMBER simulation.

RMS fluctuations in the individual helical parameters, given in parentheses in Tables 2–5, are slightly larger in the AMBER simulation for most values. With the AMBER force field the whole conformational space between canonical B- and A-DNA is accessible, while the CHARMM force field only rarely reaches canonical B-DNA values.

A comparison with the crystallographic data shows surprisingly good agreement of the cytosine/guanine tract in the CHARMM simulation in most helical parameters. The helical rise is somewhat smaller, with 2.77 Å compared to 3.0 Å in the crystal data, and the propeller twist is found to be less pronounced in the simulation. The cytosine/guanine averages from the AMBER simulation are comparable to the experimental structures, but do not agree as well as CHARMM for most values. The helix is underwound with a twist angle of only 28.8° compared to the experimental 32.7°, and the orientation of the basepairs with respect to the helical axis differs notably in inclination, tip, and displacement along the long (y) axis.

In the thymine/adenine tract neither simulation can satisfactorily reproduce the experimentally expected geometries in B-DNA form. However, x displacement, slide, and inclination are closer to the B form with the AMBER force field than with CHARMM. Inclination angles are higher in both force fields in the thymine/adenine part than for the cytosine/guanine basepairs. While the simulations are different in the cytosine/guanine part, very similar average twist and rise values of 32° and 2.9–3.1 Å are observed in both

TABLE 3   Individual average inter-basepair parameters in CHARMM simulation

Pairs	Roll	Tilt	Slide	Rise	Twist
CG/CG 2–3	3.9 (4.3)	−2.3 (2.4)	−1.7 (0.31)	2.8 (0.35)	31.0 (3.2)
CG/CG 3–4	3.9 (4.2)	−1.5 (2.4)	−1.7 (0.31)	2.8 (0.34)	31.3 (3.4)
CG/CG 4–5	4.7 (4.3)	−1.2 (2.5)	−1.8 (0.30)	2.6 (0.31)	31.9 (3.1)
CG/TA 5–6	2.4 (4.1)	0.4 (2.2)	−1.5 (0.39)	2.9 (0.33)	31.7 (2.5)
TA/TA 6–7	5.3 (4.7)	1.1 (2.4)	−1.5 (0.40)	2.9 (0.33)	31.8 (2.5)
TA/TA 7–8	6.9 (4.8)	2.4 (2.7)	−1.5 (0.42)	2.8 (0.34)	32.4 (2.5)
TA/TA 8–9	6.8 (5.0)	2.9 (2.7)	−1.4 (0.43)	2.8 (0.37)	32.8 (2.8)

Standard deviations from all datapoints between 4 and 10 ns are given in parentheses.

TABLE 4 Individual average base-axis and intrabase parameters in AMBER simulation

Pair	Inclination	Tip	x Displacement	y Displacement	Propeller	Buckle
CG 2	5.6 (5.3)	−2.5 (6.5)	−4.1 (0.97)	0.81 (0.84)	−4.8 (7.7)	5.4 (9.6)
CG 3	4.0 (4.7)	−1.5 (5.3)	−4.0 (0.94)	0.80 (0.67)	−2.6 (7.1)	3.1 (9.2)
CG 4	3.0 (4.4)	−0.1 (4.4)	−3.8 (0.91)	0.81 (0.64)	−3.0 (6.9)	2.0 (9.3)
CG 5	3.4 (4.2)	1.5 (4.3)	−3.5 (0.94)	0.67 (0.62)	−3.1 (7.0)	−2.5 (8.7)
TA 6	5.5 (4.1)	−0.6 (4.0)	−3.3 (0.97)	0.50 (0.61)	−8.9 (7.5)	−4.3 (9.6)
TA 7	5.7 (4.7)	−4.3 (4.9)	−3.1 (1.13)	0.75 (0.74)	−12.1 (7.7)	−3.6 (11.4)
TA 8	4.6 (5.6)	−5.6 (5.3)	−2.9 (1.11)	0.98 (0.87)	−14.4 (7.9)	−5.6 (11.2)
TA 9	3.8 (6.2)	−5.6 (6.3)	−2.3 (1.47)	1.33 (1.13)	−13.4 (8.8)	−10.3 (12.8)

Standard deviations from all datapoints between 4 and 10 ns are given in parentheses.

simulations compared to 36° twist and 3.2 Å rise expected from experiment.

Both force fields model a larger propeller twist in the thymine/adenine tract expected from experimental data (Alexeev et al., 1987; Coll et al., 1987; Nelson et al., 1987). For the buckle angle we find a similar large positive angle in the cytosine/guanine part for the CHARMM force field, but a slightly negative value close to the experiment for AMBER. The large buckle angle in the CHARMM simulation can be explained by the heteronomous backbone conformation detailed below.

Roll and tilt angles between successive basepairs describe bending of DNA toward the major and minor grooves (positive and negative roll, respectively) and the backbone (tilt) (Lavery and Sklenar, 1989). The double helix structure favors bending toward the grooves (Young et al., 1995). Curvature in longer DNA helices is explained by DNA segments with different roll angles or bent and straight segments in appropriate phase with respect to a full helical turn (Marini et al., 1982; Trifonov, 1986; Calladine et al., 1988; Crothers et al., 1990; Hagerman, 1994; Goodsell and Dickerson, 1994).

Fig. 5 shows the average roll angles along the simulated helix for both force fields together with the individual RMS fluctuations. While both force fields produce constant roll angles of 4° along the cytosine/guanine basepairs the result for the thymine/adenine part is quite different. With CHARMM parameters roll values increase to 6° after a small drop to 2° at the C-T junction. However, the AMBER force field shows a straight thymine/adenine tract with average roll angles close to zero, in good agreement with single crystal data. Small average tilt angles are similar with both force fields and comparable to crystal data.

Backbone

Between the third and fourth adenine bases the backbone of the first AMBER simulation assumes a conformation at 1.5 ns with $\alpha = 80°$, $\gamma = 186°$, $\beta = 216°$, $\epsilon = 277°$, and $\zeta = 141°$ usually observed only in left-handed Z-DNA structures (Dickerson, 1991) and does not return to the normal B type during the next 4.5 ns. Fig. 6 shows the adenine backbone segment in this conformation compared to the usual B_I, B_{II}, and A conformations observed in the second AMBER and CHARMM simulations. While similar to the B_{II} structure, $\alpha/\beta/\gamma$ undergo a transition from (*gauche−*, *trans*, *gauche+*) to (*gauche+*, *trans*, *gauche−*) as in the observed Z-like form.

For the second AMBER and the CHARMM simulations Table 6 shows the average backbone dihedral angles and furanose ring pseudorotations (Saenger, 1984) for each base type compared to results from crystallographic data with error values estimated in the same fashion as described above. Individual averages for each base are given in Tables 7 and 8 together with the RMS fluctuations in parentheses. A- and B-type backbones are characterized by the sugar pseudorotation angle and the correlated δ dihedral (Figs. 7 and 8). C3′-endo conformations with pseudorotations around 10° are characteristic of A-DNA, whereas O4′-endo, C1′-exo, and C2′-endo (80–180°) are observed for B-DNA. The average values indicate an overall B conformation in the AMBER simulation, but a heterogeneous backbone with the purine strand in A and the pyrimdine strand mostly in B form with CHARMM parameters. A more complete dynamical picture is given by density plots of pseudorotation angle profiles for 100-ps time windows, overlapping by 25 ps, along the trajectories in Figs. 7 and 8 showing the distribu-

TABLE 5 Individual average inter-basepair parameters in AMBER simulation

Pairs	Roll	Tilt	Slide	Rise	Twist
CG/CG 2–3	3.4 (4.8)	−0.6 (2.6)	−1.7 (0.47)	3.1 (0.46)	28.9 (3.7)
CG/CG 3–4	3.0 (4.8)	−0.6 (2.6)	−1.6 (0.52)	3.3 (0.48)	28.6 (3.6)
CG/CG 4–5	3.2 (5.0)	0.1 (2.6)	−1.7 (0.52)	3.2 (0.42)	28.9 (3.8)
CG/TA 5–6	0.2 (4.6)	1.8 (2.5)	−1.6 (0.52)	3.2 (0.39)	29.5 (3.6)
TA/TA 6–7	−0.4 (5.6)	1.6 (2.6)	−1.1 (0.60)	3.1 (0.40)	32.2 (5.1)
TA/TA 7–8	1.5 (4.9)	1.6 (2.7)	−1.0 (0.56)	3.1 (0.42)	30.9 (4.2)
TA/TA 8–9	2.3 (5.2)	2.5 (2.7)	−0.8 (0.68)	3.1 (0.39)	33.2 (4.9)

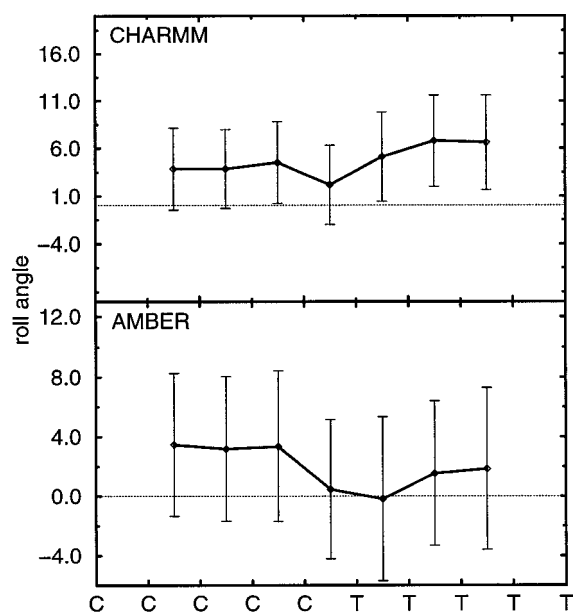Standard deviations from all datapoints between 4 and 10 ns are given in parentheses.

FIGURE 5   Average roll angle profile along base sequence in CHARMM and AMBER simulations with RMS fluctuations from 4 to 10 ns.

tion of sugar conformations over time for each base type. Table 9 quantifies the population of sugar conformations during the last 6 ns of simulation time. Similar behavior is found for all bases in the AMBER simulation. Mostly the B-type O4′-endo through C2′-endo conformations are populated, with a preference for C1′-exo, particularly in the thymine backbone. For the guanine and adenine backbone short-lived transitions to C3′-endo are occasionally observed. In the CHARMM simulation the purine backbone remains exclusively in C2′-exo/C3′-endo throughout the simulation. The opposite pyrimidine backbone is in dynam-
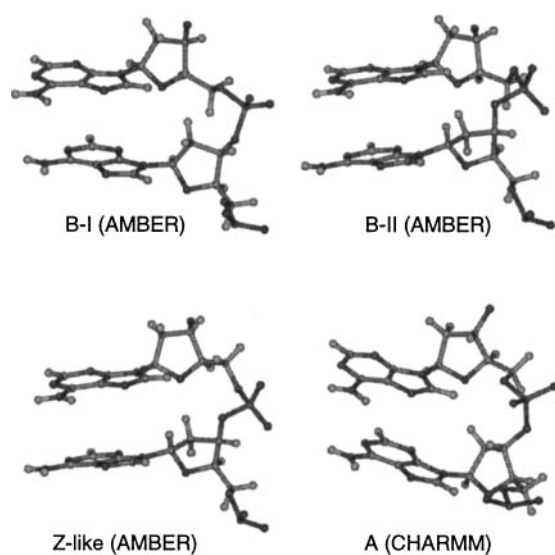

FIGURE 6   Adenine backbone in B_I, B_{II}, and Z-like conformations from AMBER simulations compared to A conformation from the CHARMM simulation. Shown are the third and fourth adenine (from the 5′ end) bases.

TABLE 6   Average backbone dihedral values compared to experimental results for each base type

Dihedral	Base	CHARMM*	AMBER*	X-ray[#§]
α	cyt	289.0 (0.03)	291.2 (0.11)	286.5 (5.9)
	thy	291.4 (0.02)	295.3 (0.08)	297.8 (8.2)
	ade	292.0 (0.02)	289.4 (0.15)	278.5 (7.5)
	gua	291.2 (0.01)	291.9 (0.05)	291.9 (4.1)
β	cyt	164.1 (0.03)	172.1 (0.11)	176.9 (4.4)
	thy	165.0 (0.02)	170.2 (0.07)	175.2 (9.1)
	ade	167.2 (0.06)	166.3 (0.26)	163.1 (7.1)
	gua	170.1 (0.03)	171.7 (0.06)	175.9 (2.1)
γ	cyt	57.3 (0.03)	57.0 (0.13)	55.9 (4.6)
	thy	59.3 (0.04)	58.4 (0.06)	49.1 (7.0)
	ade	59.2 (0.03)	54.2 (0.16)	43.6 (5.7)
	gua	61.3 (0.04)	57.5 (0.07)	67.7 (4.3)
δ	cyt	108.8 (0.11)	110.0 (0.53)	81.4 (1.5)
	thy	93.3 (0.01)	111.2 (0.21)	128.6 (9.2)
	ade	82.1 (0.01)	118.4 (0.39)	136.0 (6.5)
	gua	81.8 (0.01)	106.4 (0.30)	80.2 (1.1)
ϵ	cyt	201.7 (0.01)	189.8 (0.16)	197.6 (2.0)
	thy	205.7 (0.02)	186.0 (0.06)	184.1 (10.3)
	ade	214.1 (0.02)	201.4 (0.83)	193.0 (6.2)
	gua	210.9 (0.02)	188.5 (0.06)	208.5 (3.8)
ζ	cyt	265.0 (0.03)	271.8 (0.23)	294.9 (3.2)
	thy	277.9 (0.02)	270.7 (0.09)	225.1 (15.8)
	ade	284.5 (0.01)	250.5 (1.21)	237.8 (7.3)
	gua	286.2 (0.01)	272.9 (0.16)	289.3 (3.1)
χ	cyt	219.7 (0.06)	224.7 (0.25)	203.7 (2.8)
	thy	213.4 (0.02)	229.7 (0.16)	253.5 (6.3)
	ade	193.3 (0.01)	238.4 (0.39)	254.3 (1.2)
	gua	188.2 (0.01)	220.2 (0.23)	192.6 (1.6)
P	cyt	100.1 (0.20)	114.5 (0.89)	10.1 (6.4)
	thy	49.5 (0.02)	116.2 (0.33)	162.7 (7.6)
	ade	7.6 (0.02)	125.5 (0.63)	157.0 (4.7)
	gua	7.0 (0.01)	108.5 (0.51)	16.3 (5.5)

Statistical errors are given in parentheses for simulation averages and experimental values.
*Average calculated over 4–10 ns without edge and junction bases.
[#]C/G values averaged over six inner basepairs from crystal structures for d(CCCCGGGG)$_2$ (Haran et al., 1987) and d(GGGGCCCC)$_2$ (McCall et al., 1985).
[§]A/T values averaged over eight inner basepairs from crystal structures for d(CGCA$_5$GCG) · d(CGCT$_5$GCG) (Nelson et al., 1987) and d(CGCGA$_6$CG) · d(CGT$_6$CGCG) (Grzeskowiak et al., 1991).

ical equilibrium between A and B sugar puckers, with the cytosine part favoring B and the thymine part favoring A conformations.

The backbone conformations can be compared to the solution studies with NMR and Raman spectroscopy mentioned above. In the cytosine/guanine moiety B-DNA conformations as in the AMBER force field simulations are found experimentally (Benevides et al., 1986; Nishimura et al., 1986; Sarma et al., 1986; Rinkel et al., 1986; Wolk et al., 1989), although for lower salt concentrations than in the present simulations. A heteronomous conformation is ob-

TABLE 7 Individual average backbone dihedral angles in CHARMM simulation

Base	α	β	γ	δ	ε	ζ	χ	P
C2	288.9 (11.1)	158.1 (16.5)	56.3 (9.1)	114.0 (20.1)	202.3 (13.0)	263.0 (20.7)	225.6 (16.4)	112.1 (39.4)
C3	289.1 (10.8)	163.6 (12.7)	57.2 (8.8)	110.7 (19.9)	201.9 (12.1)	264.4 (19.4)	222.0 (16.0)	105.1 (41.3)
C4	289.0 (10.8)	164.0 (12.0)	57.3 (8.7)	107.0 (21.7)	200.9 (10.9)	267.7 (18.1)	217.5 (16.2)	95.0 (48.3)
C5	290.1 (10.2)	164.8 (11.0)	57.5 (8.6)	95.4 (18.5)	203.2 (10.2)	274.9 (13.4)	208.3 (13.5)	66.4 (48.6)
T6	290.8 (10.2)	165.6 (10.3)	58.9 (8.3)	94.3 (18.4)	205.3 (10.7)	276.9 (13.0)	211.4 (15.0)	55.8 (50.5)
T7	291.5 (9.9)	164.0 (10.6)	59.5 (8.3)	94.0 (18.6)	205.6 (10.7)	277.7 (12.8)	213.7 (15.7)	52.6 (51.1)
T8	291.8 (10.2)	164.7 (10.6)	59.4 (8.1)	92.7 (16.9)	206.1 (10.8)	279.1 (12.6)	213.2 (15.5)	46.4 (48.1)
T9		166.4 (10.9)	59.1 (8.3)	95.4 (19.6)			217.9 (15.8)	53.1 (52.9)
A12	292.0 (9.4)	167.3 (11.8)	58.5 (8.1)	82.9 (5.4)	215.4 (10.8)	284.3 (9.1)	193.4 (7.8)	6.3 (8.7)
A13	292.1 (9.3)	166.0 (11.2)	59.4 (8.0)	82.2 (5.3)	213.0 (10.3)	284.9 (8.7)	193.3 (7.4)	7.4 (8.4)
A14	291.8 (9.1)	168.3 (10.9)	59.0 (7.9)	81.9 (5.2)	214.0 (10.2)	284.4 (8.7)	193.3 (7.4)	7.7 (8.2)
A15	290.8 (9.4)	167.2 (10.7)	59.2 (8.0)	81.4 (5.2)	216.0 (11.0)	281.4 (9.4)	192.7 (7.3)	8.1 (8.0)
G16	291.0 (9.0)	162.4 (11.4)	61.8 (8.1)	81.5 (5.1)	209.4 (8.9)	286.2 (7.7)	189.5 (6.6)	7.3 (7.7)
G17	290.8 (8.9)	171.0 (9.3)	61.0 (7.9)	81.8 (5.2)	212.1 (9.4)	286.0 (7.9)	188.3 (6.5)	6.9 (7.9)
G18	291.7 (8.9)	169.5 (9.6)	61.3 (7.8)	81.8 (5.2)	211.2 (9.1)	286.4 (7.8)	188.1 (6.5)	7.0 (8.1)
G19		169.9 (9.8)	61.7 (7.9)	82.4 (5.4)			189.5 (6.9)	7.6 (8.7)

Standard deviations are given in parentheses.

served for salt concentration of 1 M NaCl comparable to the simulation conditions (Nishimura et al., 1986). However, the guanine backbone was assigned as B form and the cytosine backbone in A form, opposite to the conformation found in the CHARMM simulation. The adenine/thymine part has been reported with a predominantly B-DNA backbone up to fairly high salt concentrations of several M NaCl (Behling and Kearns, 1986; Leijon et al., 1995; Celda et al., 1989; Searle and Wakelin, 1990). Raman studies find fractions of the thymine · backbone in A-DNA form (Thomas and Peticolas, 1983; Taillandier et al., 1987) suggesting an equilibrium between both conformations with a preference for the B-DNA backbone. The CHARMM simulation does show a similar dynamical equilibrium in the thymine backbone, tending more toward the A conformation, but the adenine backbone in A form only matches results from early fiber experiments on poly(dA) · poly(dT) (Arnott et al.,

1983). The reported heteronomous conformation with A-type C3′-endo adenine and B-type C2′-endo thymine sugar conformations is not supported by solution studies, though (Sarma et al., 1985). We have found that AMBER, however, reproduces the generally expected B conformation in both strands.

The distribution of ε-ζ dihedral angles during the last 6 ns is depicted in the contour plots in Figs. 9 and 10. While values for ε and ζ also distinguish between A and B type conformations, they differ most for transitions from B_I to the less common B_{II} backbone conformations. The B_{II} conformation involves the rotation of the phosphate group toward the minor groove resulting in a (*gauche−*, *trans*) kink conformation with ε ≈ 275 and ζ ≈ 150 (Prive et al., 1987). Fig. 6 shows a model of the B_{II} backbone in comparison with the usual B_I form. We only find the occurrence of transitions to B_{II} in the AMBER simulation. Table 10

TABLE 8 Individual average backbone dihedral angles in AMBER simulation

Base	α	β	γ	δ	ε	ζ	χ	P
C2	290.2 (10.7)	193.4 (19.5)	178.8 (40.7)	110.6 (21.1)	190.6 (9.1)	273.8 (12.9)	221.8 (16.4)	110.1 (34.8)
C3	290.9 (10.8)	173.0 (10.1)	56.9 (9.9)	110.3 (19.0)	190.1 (11.7)	271.4 (15.3)	224.7 (15.0)	114.6 (29.8)
C4	292.4 (10.5)	171.0 (10.3)	56.9 (9.8)	109.7 (18.3)	188.6 (12.7)	270.3 (18.0)	224.8 (15.6)	114.4 (27.5)
C5	294.6 (10.1)	172.1 (10.2)	57.2 (9.8)	109.9 (16.8)	186.8 (8.5)	270.5 (10.7)	221.6 (13.6)	116.0 (24.7)
T6	295.0 (10.0)	172.5 (9.5)	57.7 (9.4)	107.8 (16.8)	186.5 (8.8)	270.6 (11.2)	222.5 (13.6)	111.7 (25.8)
T7	295.8 (9.6)	170.8 (9.7)	58.7 (9.4)	111.3 (16.9)	185.4 (8.6)	270.5 (10.8)	229.7 (14.2)	116.4 (27.3)
T8	295.1 (9.7)	170.1 (9.6)	58.4 (9.3)	111.1 (16.4)	186.2 (8.4)	271.2 (10.6)	229.6 (14.3)	116.0 (26.2)
T9		169.6 (9.5)	58.1 (9.4)	109.1 (17.3)			229.8 (14.2)	112.1 (28.7)
A12	287.8 (13.6)	167.4 (16.9)	53.5 (11.6)	127.4 (18.3)	212.4 (41.0)	233.8 (57.5)	251.3 (23.8)	138.1 (29.8)
A13	290.0 (11.7)	162.7 (19.2)	53.5 (10.5)	119.0 (19.8)	191.2 (17.1)	266.6 (23.5)	238.0 (18.3)	128.2 (31.4)
A14	290.3 (11.9)	170.0 (12.3)	54.4 (10.2)	117.7 (20.2)	200.7 (33.1)	251.2 (44.3)	238.8 (21.0)	122.9 (31.1)
A15	291.3 (10.5)	166.3 (15.3)	54.7 (10.6)	112.0 (21.1)	189.0 (12.2)	271.1 (17.5)	229.9 (17.0)	115.3 (37.3)
G16	291.4 (10.5)	170.5 (10.7)	56.0 (10.4)	108.3 (19.2)	188.6 (10.7)	271.3 (15.3)	224.6 (16.6)	111.5 (31.7)
G17	291.2 (10.5)	171.7 (10.1)	56.1 (10.1)	104.8 (20.2)	189.3 (9.2)	274.0 (13.9)	219.6 (16.4)	105.8 (34.1)
G18	293.2 (10.1)	171.5 (9.7)	57.7 (10.1)	108.0 (20.0)	187.5 (8.5)	273.4 (11.9)	220.8 (16.3)	111.1 (33.3)
G19		174.2 (10.6)	58.6 (19.8)	106.6 (19.3)			218.2 (15.4)	107.9 (32.7)

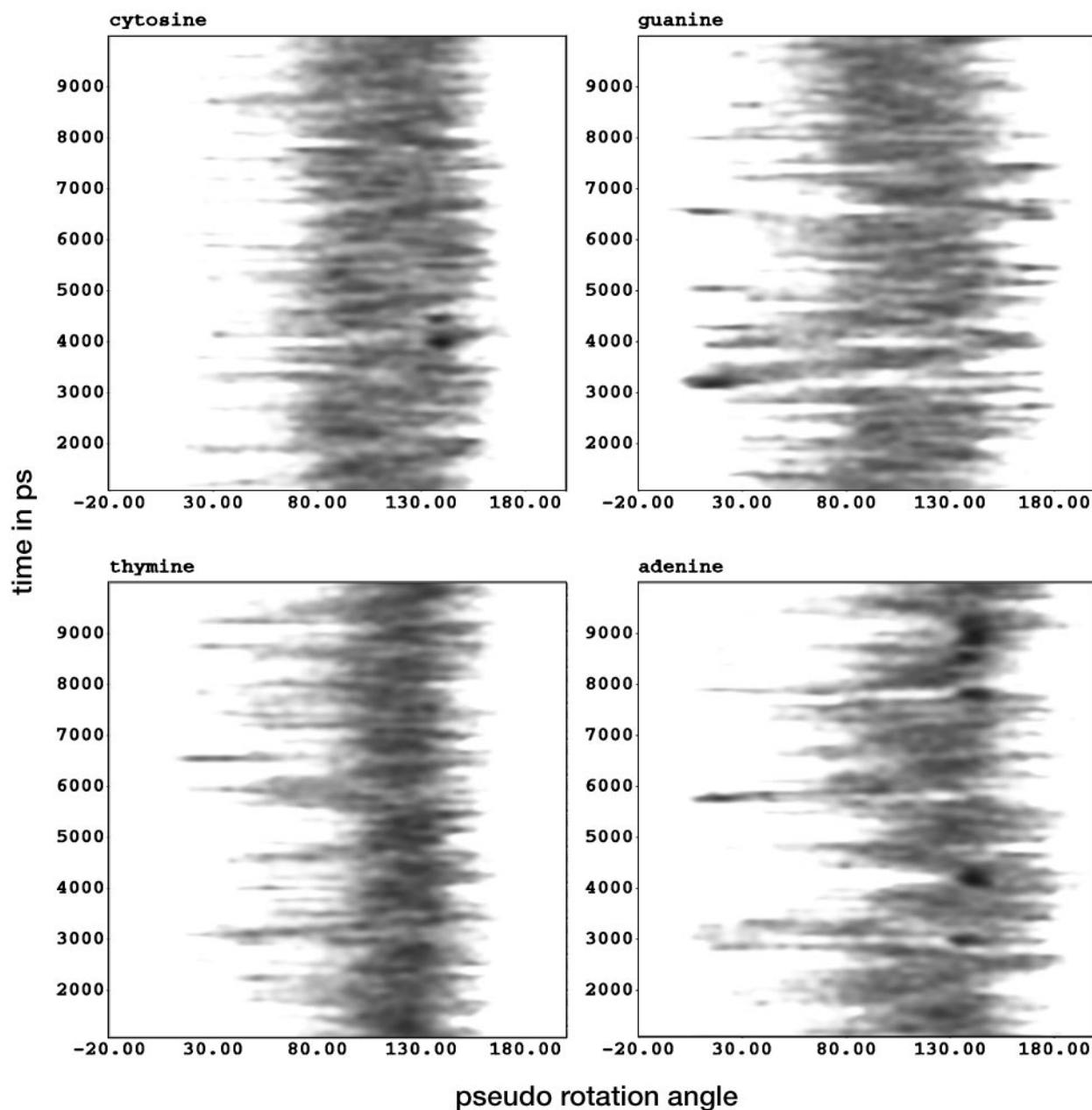Standard deviations are given in parentheses.

FIGURE 7　Time-dependent sugar pseudorotation angle distribution profiles for cytosine, guanine, thymine, and adenine backbones in AMBER simulation (see text).

gives the population of B_{II} conformations and shows that 18% of all adenine backbone conformations are found in B_{II}, but only 0.5% of the guanine and cytosine and none of the thymine backbone conformations. In Table 6 a comparison of average ϵ and ζ values with the results from crystal data shows more similar values and trends in the AMBER simulation than in the CHARMM simulation. This seems to indicate that a dynamical equilibrium between B_I and B_{II} conformations as modeled by the AMBER force is a good reflection of the observed behavior.

Comparison of the other dihedrals exhibits notable differences between the CHARMM and AMBER force fields for β in the pyrimidine backbone and for γ in the purine

backbone, but the AMBER results are generally somewhat closer to the experimental crystal values. Smaller χ angles in the adenine/guanine strand from the CHARMM simulation are expected for the observed A backbone conformation.

DISCUSSION

Our results demonstrate that long-time molecular dynamics of nucleic acid segments produce stable and reasonable structures with the current AMBER and CHARMM force fields with the Ewald summation technique for calculation of electrostatic interactions. We have used these resulting structures to make detailed comparisons with the experiment.
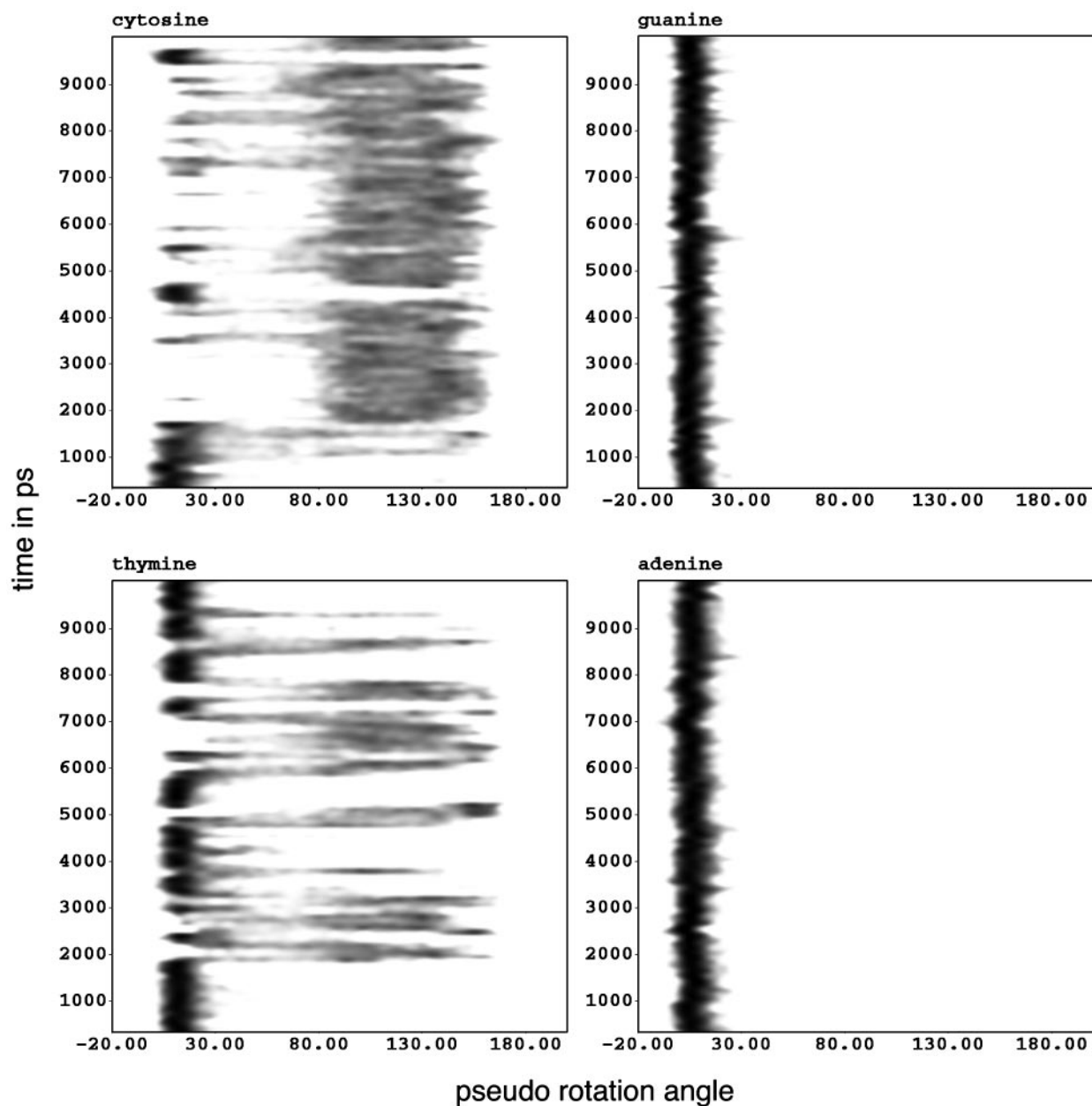
FIGURE 8 Time-dependent sugar pseudorotation angle distribution profiles for cytosine, guanine, thymine, and adenine backbones in CHARMM simulation (see text).

Simulation times of 10 ns reveal fluctuations between A and B conformations over several nanoseconds in both force fields. Corresponding DNA dynamics (Barkley and Zimm,

TABLE 9 Distribution of furanose ring populations in CHARMM/AMBER simulations in percent

Base	C2′-exo	C3′-endo	O4′-endo	C1′-exo	C2′-endo	Other
Cytosine	0.7/0.0	13.8/0.9	27.2/32.1	38.5/45.0	14.3/15.3	5.5/6.8
Guanine	18.6/0.3	81.3/5.3	0.0/32.2	0.0/36.7	0.0/12.9	0.1/12.6
Adenine	17.5/0.1	82.3/1.5	0.0/19.6	0.0/45.8	0.0/25.9	0.2/7.1
Thymine	3.0/0.0	58.8/1.0	11.1/24.8	12.9/55.3	5.7/12.2	8.4/6.7

C2′-exo: −36–0; C3′-endo: 0–36; O4′-endo: 72–108; C1′-exo: 108–144; C2′-endo: 144–180.

1979; Mirau et al., 1985) were observed recently with correlation times of 2.5 ns in electron paramagnetic resonance experiments of short DNA fragments (Keyes et al., 1997) and 3–4 ns for a 10-basepair fragment in NMR measurements of cytosine H6-H5 cross correlations (Lane, 1995). Initial convergence times necessary to arrive at dynamical equilibrium in all structural quantities were estimated to be on the same order, around 4 ns, corresponding also with the formation and equilibration of the ion atmosphere around the DNA solute from ions initially placed at random with measured diffusion constants (V. Makarov, M. Feig, and B. M. Pettitt, submitted for publication). This brings a new perspective to previously reported conformational transitions in the sequences d(CGCGAATTCGCG)$_2$
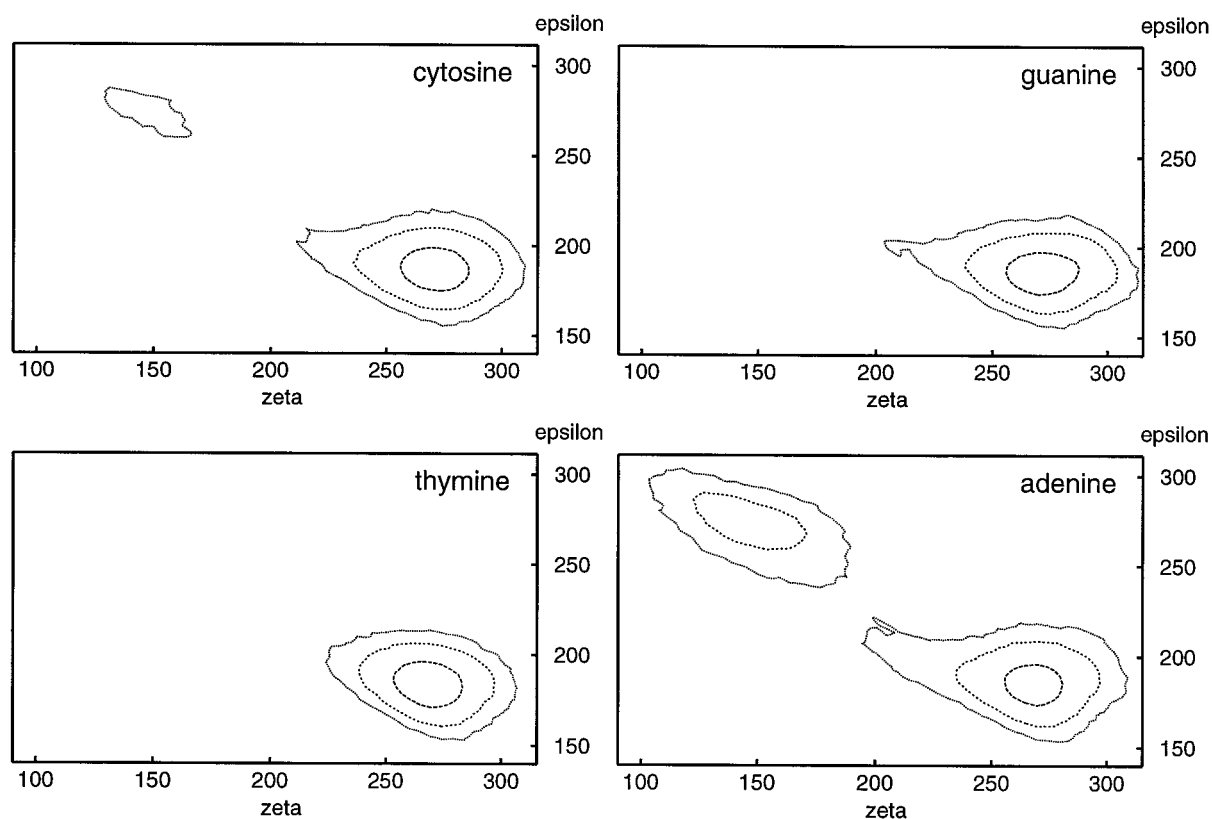
FIGURE 9   Distribution of ϵ/ζ dihedrals for cytosine, guanine, thymine, and adenine backbones in AMBER simulation.

and d(CCAACGTTGG)$_2$ to A and B structures after 1.5 and 3.5 ns for the CHARMM and AMBER force fields, respectively (Yang and Pettitt, 1996; Cieplak et al., 1997; Cheatham and Kollman, 1996). We find typical B-DNA structures at 1.5 and 2.5 ns in the first and second AMBER simulations, respectively, close to the reported "converged" B conformations in four AMBER simulations from another laboratory after 1.5 ns (Cheatham and Kollman, 1996). In a longer 5-ns simulation of d(CGCGAATTCGCG)$_2$ with the AMBER force field by Young et al. (1997) the DNA helix remained closer to B-DNA than A-DNA throughout almost all of the simulation time. While the simulations by Cheatham et al. (1995), Cheatham and Kollman (1996), Cieplak et al. (1997), and Young et al. (1997) were performed with only counterions and no additional salt, the 0.8 M added salt in our simulations might explain an average structure intermediate between A and B with fluctuations between both conformations in the AMBER simulation. This generally agrees with the expectation of a conformational shift toward A-DNA in higher salt concentrations. However, a larger shift toward A-DNA in the A-philic C/G part than in the B-philic A/T tract (Ivanov and Minchenkova, 1995), as would be expected from experimental data (Ivanonv et al., 1996; Wang et al., 1989), is not observed in our simulation. Further studies will be necessary to better understand the salt influence on DNA conformation in molecular dynamics simulations.

On average, the CHARMM force field produces A-DNA base geometries with the purine backbone in A conformation and the pyrimidine backbone in dynamical equilibrium between A and B forms. For the AMBER force field the base geometries are also in A form for the cytosine/guanine moiety and intermediate between A and B, but closer to the A conformation, in the thymine/adenine half. The backbone is B type on both strands with 18% B$_{II}$ conformations at the adenine bases.

Experimental data from crystal diffraction are particularly well reproduced in the base geometries of the cytosine/guanine part by the CHARMM force field. Agreement with experiment in the thymine/adenine part is better with the AMBER force field, but only satisfactory in reproducing high propeller twist angles, small negative buckle, and roll angles close to zero, since neither simulation generates the B form found from crystallographic data. However, a comparison with recent linear dichroism studies on poly(dA) · poly(dT) (Yamaoka et al., 1997) under solution conditions that resemble the simulation conditions better than the crystal environment shows experimental findings of A-like inclined bases, a 3-Å helical rise, and roll and tilt angles of opposite sign as produced in both simulations. Note that the observed positive tilt in the thymine/adenine part changes sign for adenine/thymine basepairs. Linear and circular dichroism studies on poly(dC) · poly(dG) in solution (Kang and Johnson, 1994; Edmondson and Johnson, 1986) also
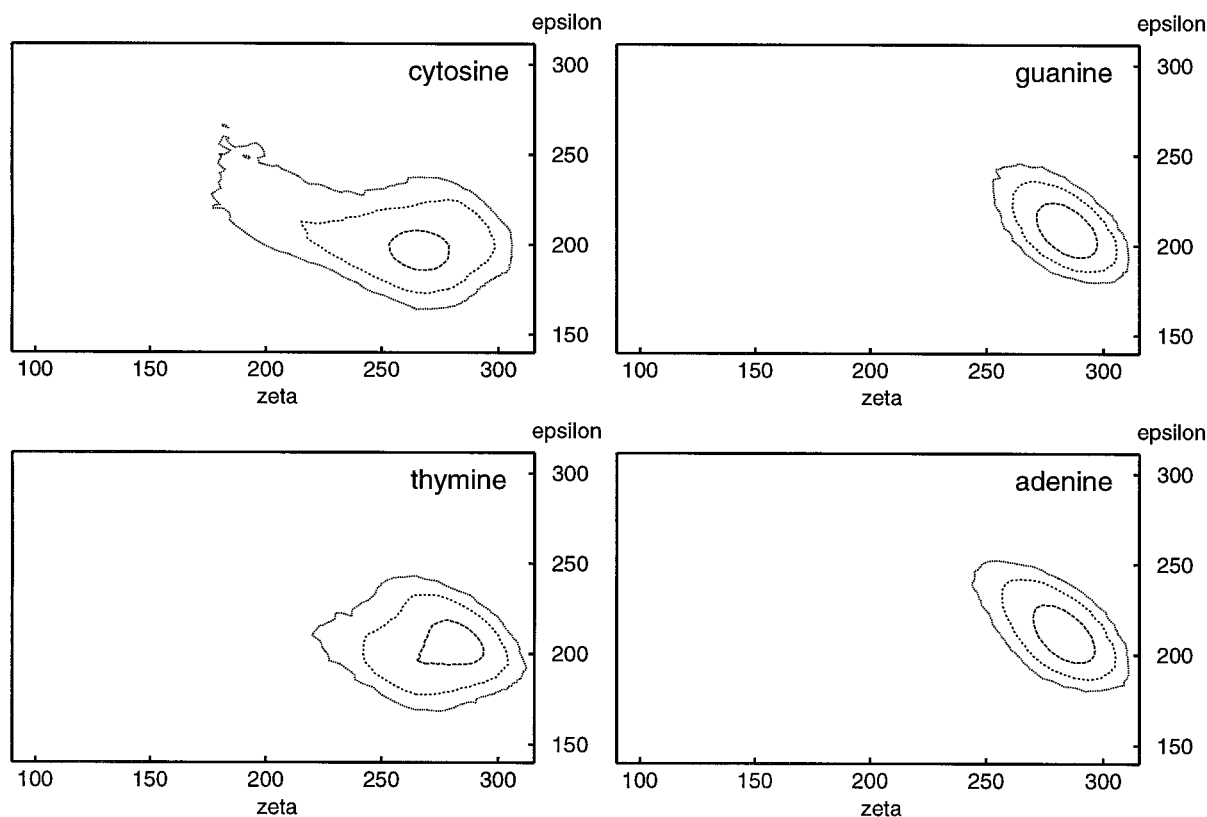
FIGURE 10   Distribution of ϵ/ζ dihedrals for cytosine, guanine, thymine, and adenine backbones in CHARMM simulation.

find highly inclined bases in agreement with the simulated structures.

Zero roll angles in the thymine/adenine tract and positive roll angles of 4° in the cytosine/guanine basepairs, as found with the AMBER force field, correspond well with the bending models by Calladine et al. (Calladine and Drew, 1986; Calladine et al., 1988) and Goodsell et al. (Goodsell et al., 1994), which assume straight A-tracts and bent non-A-tracts with positive roll. These result in an AMBER simulation that appears bent toward the major groove around the C/T-junction, as expected from experiment (Wang et al., 1989; Ivanonv et al., 1996).

The CHARMM parameters also produce the cytosine/guanine roll angles of 4°, but generate even larger roll of 6° for the thymine/adenine tract. Thus significant bending is not introduced at the C/T junction resulting in structures that are inconsistent with bending models explaining DNA curvature (Crothers et al., 1990; Hagerman, 1990; Goodsell and Dickerson, 1994).

TABLE 10   Percentage of B_{II} backbone population with $\epsilon \approx 275°$ and $\zeta \approx 150°$ in AMBER simulation

Base	%B_{II}
Cytosine	0.36
Guanine	0.58
Adenine	18.41
Thymine	0.005

The modeling of the backbone in B conformation with the AMBER parameters does correspond to Raman and NMR data, although a larger population of sugar rings in A conformation has been reported for the simulated salt concentration of ~1 M. Experimental evidence for B_{II} conformations is only available from crystal studies of DNA sequences (Prive et al., 1987; Heinemann and Alings, 1989) and cannot be easily distinguished from the canonical B_{I} form in NMR spectroscopy (Hartmann et al., 1983). Although the average ϵ and ζ angles—including those from B_{II} conformations—are comparable to the average structures from x-ray diffraction, it is not clear whether frequent transitions, as modeled by the simulation, actually occur in general DNA sequences in solution (Hartmann et al., 1983; Dickerson et al., 1987; Jain and Sundaralingam, 1989).

Interestingly, the first AMBER simulation displays a transition to a backbone conformation typically found in Z-like structures. In a recent extensive analysis of DNA sugar-phosphate backbone conformations from available crystallographic data (Schneider et al., 1997) few residues in B-DNA structures are also found with a similar conformation with $\alpha \approx 50°$. While a B to Z transition is not expected to be completed for the sequence studied, it could constitute the first step in a transition toward Z-DNA conformation that is favored by high salt environments (Saenger, 1984).

The heterogeneous backbone conformation in the CHARMM force field does not agree with experimental

data indicating a parametrization problem for the backbone with purines that never deviates from the C2′-exo/C3′-endo conformations throughout the whole simulation.

Coexistence of A/B type backbone structures with different helix conformations has been discussed before (Edmondson, 1987). In our simulations the DNA helix is not in a uniform A or B conformation in either bases or backbone. This addresses the important question on the influence of the backbone on base orientations, which ultimately define the helix geometry as A or B form. While previous theoretical studies have concluded that the backbone conformation drives the helix geometry (Tung and Soumpasis, 1996), we find that an all-B form backbone does not induce full B type base geometries in the AMBER simulation, and a mostly B form cytosine backbone in the CHARMM simulation is observed with A type base geometries. Correlations can be found for fluctuations between A and B structures in the sugar pseudorotation dynamics in Fig. 7 and the time series of inclination and rise in Fig. 3.

It remains to be seen how force field improvements on the backbone (A. MacKerell, private communication) and the inclusion of polarization effects (Kollman, 1996) will affect the structure and dynamics of nucleic acid simulations. This study focuses on the solute structure alone, but DNA structure and dynamics are influenced by its interaction with the aqueous ionic environment. A subsequent analysis of solute dynamics, solvent structure, and the effect of ionic concentration will complete the picture of nucleic acid structure and dynamics obtained from molecular dynamics simulations on the 10-ns time scale.

REFERENCES

Alexeev, D. G., A. A. Lipanov, and I. Y. Skuratovskii. 1987. Poly(dA) poly(dT) is a B-type double helix with a distinctively narrow minor groove. *Nature.* 325:821–823.

Allen, M. P., and D. J. Tildesley. 1987. Computer Simulation of Liquids. 1st ed. Oxford University, New York.

Arnott, S., R. Chandrasekaran, I. H. Hall, and L. C. Puigjaner. 1983. Heteronomous DNA. *Nucleic Acids Res.* 11:4141–4155.

Auffinger, P., and D. L. Beveridge. 1995. A simple test for evaluating the truncation effects in simulations of systems involving charged groups. *Chem. Phys. Lett.* 234:413–415.

Auffinger, P., and E. Westhof. 1996. H-bond stability in the tRNA[Asp] anticodon hairpin: 3 ns of multiple molecular dynamics simulations. *Biophys. J.* 71:940–954.

Babcock, M. S., and W. K. Olson. 1994. The effect of mathematics and coordinate system on comparability and dependencies of nucleic acid structure parameters. *J. Mol. Biol.* 237:98–124.

Babcock, M. S., E. P. D. Pednault, and W. K. Olson. 1994. Nucleic acid structure analysis: mathematics for local Cartesian and helical structure parameters that are truly comparable between structures. *J. Mol. Biol.* 237:125–156.

Barkley, M. D., and B. H. Zimm. 1979. Theory of twisting and bending of chain macromolecules: analysis of the fluorescence depolarization of DNA. *J. Chem. Phys.* 70:2991–3007.

Behling, R. W., and D. R. Kearns. 1986. [1]H two-dimensional nuclear Overhauser effect and relaxation studies of poly(dA)poly(dT). *Biochemistry.* 25:3335–3346.

Benevides, J. M., A. H.-J. Wang, A. Rich, Y. Kyogoku, G. A. van der Marel, J. H. van Boom, and G. J. Thomas. 1986. The Raman spectra of single crystals of r(GCG)d(CGC) and d(CCCCGGGG) as model for A-DNA, their structure transitions in aqueous solution and comparison with double helical poly(dG) · poly(dC). *Biochemistry.* 25:41–50.

Beveridge, D. L., K. J. McConell, R. Nirmala, M. A. Young, S. Vijayakumar, and G. Ravishanker. 1994. Recent progress in molecular dynamics simulations of DNA and protein-DNA complexes including solvent. *ACS Symposium Series.* 568:381–394.

Boettcher, B. 1990. Transcription initiation and nuclease-sensitive sites upstream of the ϵ-Globin gene in K562 cells are related to poly(dA) · poly(dT) sequences. *J. Theor. Biol.* 146:333–339.

Brahms, S., and J. G. Brahms. 1990. DNA with adenine tracts contains poly(dA)-poly(dT) conformational features in solution. *Nucleic Acids Res.* 18:1559–1564.

Buckin, V. A., B. I. Kankiya, and A. P. Sarvazyan. 1989. Acoustical investigation of poly(dA) poly(dT), poly[d(A-T)] poly[d(A-T)], poly(A) poly(U) and DNA hydration in dilute aqueous solutions. *Nucleic Acids Res.* 17:4189–4203.

Calladine, C. R., and H. R. Drew. 1986. Principles of sequence-dependent flexure of DNA. *J. Mol. Biol.* 192:907–918.

Calladine, C. R., H. R. Drew, and M. J. McCall. 1988. The intrinsic curvature of DNA in solution. *J. Mol. Biol.* 201:127–137.

Celda, B., H. Widmer, and W. Leupin. 1989. Conformational studies of d(AAAAATTTTT)$_2$ using constraints from nuclear Overhauser effects and from quantitative analysis of the cross-peak fine structures in two-dimensional [1]H-nuclear magnetic resonance spectra. *Biochemistry.* 28: 1462–1471.

Chalikian, T. V., G. E. Plum, and K. J. Breslauer. 1994. Influence of drug binding on DNA hydration: acoustic and densimetric characterizations of netropsin binding to the poly(dAdT) · poly(dAdT) and poly(dA) · (dT) duplexes and the poly(dT) · poly(dA) · poly(dT) triplex at 25°C. *Biochemistry.* 33:8629–8640.

Cheatham, T. E., and P. A. Kollman. 1996. Observation of the A-DNA to B-DNA transition during unrestrained molecular dynamics in aqueous solution. *J. Mol. Biol.* 259:434–444.

Cheatham, T. E., J. L. Miller, T. Fox, T. A. Darden, and P. A. Kollman. 1995. Molecular dynamics simulations on solvated biomolecular systems: the particle mesh Ewald methods leads to stable trajectories of DNA, RNA, and proteins. *J. Am. Chem. Soc.* 117:4193–4194.

Cieplak, P., T. E. Cheatham, and P. A. Kollman. 1997. Molecular dynamics simulations find that 3′, phosphoramidate modified DNA duplexes undergo a B to A transition and normal DNA duplexes an A to B transition. *J. Am. Chem. Soc.* 119:6722–6730.

Coll, M., C. A. Frederick, A. H.-J. Wang, and A. Rich. 1987. A bifurcated hydrogen-bonded conformation in the d(AT) base pairs of the DNA dodecamer d(CGCAAATTTGCG) and its complex with distamycin. *Proc. Natl. Acad. Sci. USA.* 84:8385–8389.

Cornell, W. D., P. Cieplak, C. I. Bayly, I. R. Gould, K. M. Merz, D. M. Ferguson, D. C. Spellmeyer, T. Fox, J. W. Caldwell, and P. A. Kollman. 1995. A second generation force field for the simulation of proteins, nucleic acids, and organic molecules. *J. Am. Chem. Soc.* 117: 5179–5197.

Crothers, D. M., T. E. Haran, and J. G. Nadeau. 1990. Intrinsically bent DNA. *J. Biol. Chem.* 265:7093–7096.

D., D. A., and T. A. Steitz. 1993. A DNA dodecamer containing an adenine tract crystallizes in a unique lattice and exhibits a new band. *J. Mol. Biol.* 231:1024–1039.

de Leeuw, S. W., J. W. Perram, and E. R. Smith. 1980. Simulation of electrostatic systems in periodic boundary conditions. I. Lattice sums and dielectric constants. *Proc. R. Soc. Lond. A.* 373:27–56.

DeSantis, P., A. Palleschi, M. Savino, and A. Scipioni. 1990. Validity of the nearest-neighbor approximation in the evaluation of the electrophoretic manifestations of DNA curvature. *Biochemistry.* 29: 9269–9273.

Dickerson, R. E. 1991. DNA structure from A to Z. *Methods Enzymol.* 211:67–111.

Dickerson, R. E. 1992. NEWHELIX program suite. University of California at Los Angeles.

Dickerson, R. E., D. S. Goodsell, M. L. Kopka, and P. E. Pjura. 1987. The effect of crystal packing on oligonucleotide crystal structures. *J. Biomol. Struct. & Dyn.* 5:557–579.

Dickerson, R. E., D. S. Goodsell, and S. Neidle. 1994. ". . . the tyranny of the lattice . . ." *Proc. Natl. Acad. Sci. USA.* 91:3579–3583.

Dickerson, R. E 1989. Definitions and nomenclature of nucleic acid structure parameters. *J. Mol. Biol.* 205:787–791.

DiGabriele, A. D., M. R. Sanderson, and T. A. Steitz. 1989. Crystal lattice packing is important in determining the bend of a DNA dodecamer containing an adenine tract. *Proc. Natl. Acad. Sci. USA.* 86:1816–1820.

Duan, Y., P. Wilkosz, M. Crowley, and J. M. Rosenberg. 1997. Molecular dynamics simulation study of DNA dodecamer d(CGCGAATTCGCG) in solution: conformation and hydration. *J. Mol. Biol.* 272:553–572.

Edmondson, S. P. 1987. Polynucleotide base-pair orientation in solution: linear dichroism and molecular mechanical studies of poly[d(A)]-poly[d(T)]. *Biopolymers.* 26:1941–1956.

Edmondson, S. P., and W. C. Johnson. 1986. Base tilt of B-form poly[d(G)]-poly[d(C)] and the B- and Z-conformations of poly[d(GC)]-poly[d(GC)] in solution. *Biopolymers.* 25:2335–2348.

Edwards, K. J., D. G. Brown, N. Spink, and S. Neidle. 1992. Molecular structure of the B-DNA dodecamer d(CGCAAATTTGCG)$_2$: an examination of propeller twist and minor-groove water structure at 2.2 Å resolution. *J. Mol. Biol.* 226:1161–1173.

El Hassan, M. A., and C. R. Calladine. 1995. The assessment of the geometry of dinucleotide steps in double-helical DNA: a new local calculation scheme. *J. Mol. Biol.* 251:648–664.

Ewald, P. P. 1921. Die Berechnung optischer und elektrostatischer Gitterpotentiale. *Ann. Physik.* 64:253–287.

Fairall, L., S. Martin, and D. Rhodes. 1989. The DNA binding site of the *Xenopus* transcription factor IIIA has a non-B-form structure. *EMBO J.* 8:1809–1817.

Feig, M., and B. M. Pettitt. 1997. Experiment vs. force fields: DNA conformation from molecular dynamics simulations. *J. Phys. Chem. B.* 101:7361–7363.

Friedberg, R., and J. E. Cameron. 1970. Test of the Monte Carlo method: fast simulation of a small Ising lattice. *J. Chem. Phys.* 52:6049–6058.

Goodsell, D. S., and R. E. Dickerson. 1994. Bending and curvature calculations in B-DNA. *Nucleic Acids Res.* 22:5497–5503.

Goodsell, D. S., M. Kaczor-Grzeskowiak, and R. E. Dickerson. 1994. The crystal structure of C-C-A-T-T-A-A-T-G-G: implications for bending of B-DNA at T-A steps. *J. Mol. Biol.* 239:79–96.

Grzeskowiak, K., K. Yanagi, G. G. Prive, and R. E. Dickerson. 1991. The structure of B-helical C-G-A-T-C-G-A-T-C-G and comparison with C-C-A-A-C-G-T-T-G-G. *J. Biol. Chem.* 266:8861–8883.

Hagerman, P. J. 1990. Sequence-directed curvature of DNA. *Annu. Rev. Biochem.* 59:755–781.

Hagerman, P. J. 1994. Straightening out the bends in curved DNA. *Biochim. Biophys. Acta.* 1131:125–132.

Haran, T. E., J. D. Kahn, and D. M. Crothers. 1994. Sequence elements responsible for DNA curvature. *J. Mol. Biol.* 244:135–143.

Haran, T. E., Z. Shakked, A. H.-J. Wang, and A. Rich. 1987. The crystal structure of d(CCCCGGGG): a new A-form variant with an extended backbone conformation. *J. Biomol. Struct. & Dyn.* 5:199–217.

Hartmann, B., D. Piazzola, and R. Lavery. 1983. B$_I$-B$_{II}$ transitions in B-DNA. *Nucleic Acids Res.* 21:561–568.

Heinemann, U., and C. Alings. 1989. Crystallographic study of one turn of G/C-rich B-DNA. *J. Mol. Biol.* 210:369–381.

Herbeck, R., T. J. Yu, and W. L. Peticolas. 1976. Effect of cross-linking on the secondary structure of DNA. I. Cross-linking by photodimerization. *Biochemistry.* 15:2656–2660.

Ivanov, V. I., and L. E. Minchenkova. 1995. The A-form of DNA: in search of biological role (A review). *Mol. Biol.* 28:780–788.

Ivanonv, V. I., L. E. Minchenkova, G. Burckhardt, E. Birch-Hirschfeld, H. Fritzsche, and C. Zimmer. 1996. The detection of B-form/A-form junction in a deoxyribonucleotide duplex. *Biophys. J.* 71:3344–3349.

Iyer, V., and K. Struhl. 1995. Poly(dA:dT), a ubiquitous promoter element that stimulates transcription via its intrinsic DNA structure. *EMBO J.* 14:2570–2579.

Jacucci, G., and A. Rahman. 1984. Comparing the efficiency of Metropolis Monte Carlo and molecular dynamics methods for configuration space sampling. *Nuovo Cimento D.* 4:341–356.

Jain, S., and M. Sundaralingam. 1989. Effect of crystal packing environment on conformation of the DNA duplex. Molecular structure of the A-DNA octamer d(G-T-G-T-A-C-A-C) in two crystal forms. *J. Biol. Chem.* 264:12780–12784.

Jolles, B., A. Laigle, L. Chinsky, and P. Y. Turpin. 1985. The Poly(dA) strand of Poly(dA) · Poly(dT) adopts an A-form in solution: a UV resonance Raman study. *Nucleic Acids Res.* 13:2075–2085.

Jorgensen, W., J. Chandrasekhar, J. Madura, R. Impey, and M. Klein. 1983. Comparison of simple potential functions for simulating liquid water. *J. Chem. Phys.* 79:926–935.

Kang, H., and W. C. Johnson. 1994. Infrared linear dichroism reveals that A-, B-, and C-DNAs in films have bases highly inclined from perpendicular to the helix axis. *Biochemistry.* 33:8330–8338.

Keyes, R. S., E. V. Bobst, Y. Y. Cao, and A. M. Bobst. 1997. Overall and internal dynamics of DNA as monitored by five-atom-tethered spin labels. *Biophys. J.* 72:282–290.

Kollman, P. A. 1996. Advances and continuing challenges in achieving realistic and predictive simulations of the properties of organic and biological molecules. *Acc. Chem. Res.* 29:461–469.

Koo, H.-S., H.-W. Wu, and D. M. Crothers. 1986. DNA bending at adenine-thymine tracts. *Nature.* 320:501–506.

Lane, A. N. 1995. Determination of fast dynamics of nucleic acids by NMR. *Methods Enzymol.* 261:413–435.

Lavery, R., and H. Sklenar. 1988. The definition of generalized helicoidal parameters and of axis curvature for irregular nucleic acids. *J. Biomol. Struct. & Dyn.* 6:63–91.

Lavery, R., and H. Sklenar. 1989. Defining the structure of irregular nucleic acids: conventions and principles. *J. Biomol. Struct. & Dyn.* 6:655–667.

Lee, H., T. A. Darden, and L. Pedersen. 1995. Accurate crystal molecular dynamics simulations using particle mesh Ewald: RNA dinucleotides ApU and GpC. *Chem. Phys. Lett.* 243:229–235.

Leijon, M., J. Zdunek, H. Fritzsche, H. Sklenar, and A. Graslund. 1995. NMR studies and restrained-molecular-dynamics calculations of a long A+T-rich stretch in DNA. Effects of phosphate charge and solvent approximations. *Eur. J. Biochem.* 234:832–842.

Lindsay, S. M., S. A. Lee, J. W. Powell, T. Weidlich, C. Demarco, G. D. Lewen, N. J. Tao, and A. Rupprecht. 1988. The origin of the A to B transition in DNA fibers and films. *Biopolymers.* 27:1015–1043.

Louise-May, S., P. Auffinger, and E. Westhof. 1996. Calculations of nucleic acid conformations. *Curr. Opin. Struct. Biol.* 6:289–298.

MacKerell, A. D., Jr., J. Wiorkiewicz-Juczera, and M. Karplus. 1995. An all-atom empirical energy function for the simulation of nucleic acids. *J. Am. Chem. Soc.* 117:11946–11975.

Marini, J. C., S. D. Levene, D. M. Crothers, and P. T. Englund. 1982. Bent helical structure in kinetoplast DNA. *Proc. Natl. Acad. Sci. USA.* 79:7664–7668.

McCall, M., T. Brown, and O. Kennard. 1985. The crystal structure of d(G-G-G-G-C-C-C-C): a model for poly(dG)poly(dC). *J. Mol. Biol.* 183:385–396.

McCammon, J. A., and S. C. Harvey. 1987. Dynamics of Proteins and Nucleic Acids. Cambridge University Press, New York.

Mirau, P. A., R. W. Behling, and D. R. Kearns. 1985. Internal motions in B- and Z-form Poly(dG-dC) · Poly(dG-dC): ^{1}H-NMR relaxation studies. *Biochemistry.* 24:6200–6211.

Mooers, B. H. M., G. P. Schroth, W. W. Baxter, and P. S. Ho. 1995. Alternating and non-alternating dG-dC hexanucleotides crystallize as canonical A-DNA. *J. Mol. Biol.* 249:772–784.

Nelson, H. C. M., J. T. Finch, B. F. Luisi, and A. Klug. 1987. The structure of an oligo(dA):oligo(dT) tract and its biological implications. *Nature.* 330:221–226.

Nishimura, Y., C. Torigoe, and M. Tsuboi. 1986. Salt induced B-A transition of poly(dG) · poly(dC) and the stabilization of A form by its methylation. *Nucleic Acids Res.* 14:2737–2748.

Prive, G. G., U. Heinemann, S. Chandrasegaran, L. S. Kan, M. L. Kopka, and R. E. Dickerson. 1987. Helix geometry, hydration and GA mismatch in a B-DNA decamer. *Science.* 238:498–504.

QUANTA. 1994. Molecular Simulations Inc. Release 4.0.

Ramakrishnan, B., and M. Sundaralingam. 1993. Evidence for crystal environment dominating base sequence effects on DNA conformation: crystal structures of the orthorhombic and hexagonal polymorphs of the A-DNA decamer d(GCGGGCCCGC) and comparison with their iso-morphous crystal structures. *Biochemistry.* 32:11458–11468.

Ravishanker, G., P. Auffinger, D. R. Langley, B. Jayaram, M. A. Young, and D. L. Beveridge. 1997. Treatment of counterions in computer sim-ulations of DNA. *In* Reviews in Computational Chemistry. Vol. 11. pages 317–372.

Rinkel, L. J., M. R. Sanderson, G. A. van der Marel, and C. Altona. 1986. Conformational analysis of the octamer d(GGCCGGCC) in aqueous solution. *Eur. J. Biochem.* 159:85–93.

Ryckaert, J. P., G. Ciccotti, and H. J. C. Berendsen. 1977. Numerical integration of the Cartesian equations of motion of a system with constraints: molecular dynamics of *n*-alkanes. *J. Comput. Phys.* 23: 327–341.

Saenger, W. 1984. Principles of Nucleic Acid Structure. Springer.

Sarma, M. H., G. Gupta, and R. H. Sarma. 1986. 500-MHz ^{1}H-NMR study of poly(dG)poly(dC) in solution using one-dimensional nuclear Over-hauser effect. *Biochemistry.* 25:3659–3665.

Sarma, M. H., H. Gupta, and R. H. Sarma. 1985. Untenability of the heteronomous DNA model for poly(dA)poly(dT) in solution. This DNA adopts a right-handed B-DNA duplex in which the two strands are conformationally equivalent. A 500 MHz NMR study using one dimen-sional NOE. *J. Biomol. Struct. & Dyn.* 2:1057–1084.

Schneider, B., S. Neidle, and H. M. Berman. 1997. Conformations of the sugar-phosphate backbone in helical DNA crystal structures. *Biopoly-mers.* 42:113–124.

Schreiber, H., and O. Steinhauser. 1992. Molecular dynamics studies of solvated polypeptides: why the cut-off scheme does not work. *Chem. Phys.* 168:75–89.

Schultes, N. P. 1991. A poly(dA · dT) tract is a component of the recom-bination initiation site at the ARG4 locus in saccharomyces cerevisiae. *Mol. Cell. Biol.* 11:322–328.

Searle, M. S., and L. P. G. Wakelin. 1990. Sequence specific conformation of a DNA decamer containing an adenine tract studied in solution by ^{1}H-NMR spectroscopy. *Biochim. Biophys. Acta.* 1049:69–77.

Smith, P. E., M. E. Holder, L. X. Dang, M. Feig, and B. M. Pettitt. 1996. ESP. University of Houston.

Smith, P. E., and B. M. Pettitt. 1991. Peptides in ionic solutions: a com-parison of the Ewald and switching function techniques. *J. Chem. Phys.* 95:8430.

Smith, P. E., and B. M. Pettitt. 1994. Modeling solvent in biomolecular systems. *J. Phys. Chem.* 98:9700–9711.

Smith, P. E., and B. M. Pettitt. 1995. Efficient Ewald electrostatic calcu-lations for large systems. *Comput. Phys. Commun.* 91:339–344.

Sprous, D., W. Zacharias, Z. A. Wood, and S. C. Harvey. 1995. Dehydrat-ing agents sharply reduce curvature in DNAs containing A-tracts. *Nu-cleic Acids Res.* 23:1816–1821.

Steinbach, P. J., and B. R. Brooks. 1994. New spherical-cutoff methods for long-range forces in macromolecular simulation. *J. Comput. Chem.* 15:667–683.

Taillandier, E., J.-P. Ridoux, J. Liquier, W. Leupin, W. A. Denny, Y. Wang, G. A. Thomas, and W. I. Peticolas. 1987. Infrared and Raman studies show that poly(dA)poly(dT) and d(AAAAATTTTT)$_2$ exhibit a heteronomous conformation in films at 75% relative humidity and a B-type conformation at high humidities and in solution. *Biochemistry.* 26:3361–3368.

Thomas, G. A., and W. L. Peticolas. 1983. Fluctuations in nucleic acid conformations. 2. Raman spectroscopic evidence of varying ring pucker in A-T polynucleotides. *J. Am. Chem. Soc.* 105:993–996.

Trifonov, E. N. 1986. Curved DNA. *CRC Crit. Rev. Biochem.* 19:89–106.

Tung, C.-S., and D. M. Soumpasis. 1996. Structural prediction of A- and B-DNA duplexes based on coordinates of the phosphorus atoms. *Bio-phys. J.* 70:917–923.

Vorlickova, M., J. A. Subirana, J. Chladkova, I. Tejralova, T. Huynh-Dinh, L. Arnold, and J. Kypr. 1996. Comparison of the solution and crystal conformations of (G+C)-rich fragments of DNA. *Biophys. J.* 71: 1530–1538.

Wang, Y., G. A. Thomas, and W. L. Peticolas. 1989. A duplex of the oligonucleotides d(GGGGGTTTTT) and d(AAAAACCCCC) forms an A to B conformational junction in concentrated salt solutions. *J. Biomol. Struct. & Dyn.* 6:1177–1187.

Weerasinghe, S., P. E. Smith, V. Mohan, Y.-K. Cheng, and B. M. Pettitt. 1995. Nanosecond dynamics and structure of a model DNA triple helix in saltwater solution. *J. Am. Chem. Soc.* 117:2147–2158.

Wolk, S., W. N. Thurmes, W. S. Ross, C. C. Hardin, and I. Tinoco. 1989. Conformational analysis of d(C$_3$G$_3$), a B-family duplex in solution. *Biochemistry.* 28:2452–2459.

Yamaoka, K., N. Ojima, and Y. Fujita. 1997. Pulsed electric linear dichro-ism of double-stranded antiparallel poly(rA) · poly(rU) and poly(dA) · poly(dT) helices in solution. *J. Phys. Chem.* 101:1419–1428.

Yanagi, K., G. G. Prive, and R. E. Dickerson. 1991. An analysis of local helix geometry in three B-DNA decamers and eight dodecamers. *J. Mol. Biol.* 217:201–214.

Yang, L., and B. M. Pettitt. 1996. B to A transition of DNA on the nanosecond time scale. *J. Phys. Chem.* 100:2564–2566.

Young, M. A., G. Ravishanker, and D. L. Beveridge. 1997. A 5-nanosec-ond molecular dynamics trajectory for B-DNA: analysis of structure, motions, and solvation. *Biophys. J.* 73:2313–2336.

Young, M. A., G. Ravishanker, D. L. Beveridge, and H. M. Berman. 1995. Analysis of local helix bending in crystal structures of DNA oligonu-cleotides and DNA-protein complexes. *Biophys. J.* 68:2454–2468.